Intrinsic Century-Scale Variability in Tropical Pacific Sea Surface Temperatures and their Influence on Southwestern US Hydroclimate

Authors: Colin P. Evans[1*], Toby R. Ault[1], Sloan Coats[2], Carlos M. Carrillo[1], Xiaolu, Li[1], Marc J. Alessi[3], Dimitris A. Herrera[4], and Brandon N. Benton[5]

[1]Department of Earth and Atmospheric Sciences, Cornell University, Ithaca, NY.

[2]Department of Earth Sciences, University of Hawaii, Honolulu, HI.

[3]Department of Atmospheric Science, Colorado State University, Fort Collins, CO

[4]Instituto Geográfico Universitario, Universidad Autónoma de Santo Domingo, Santo Domingo, Dominican Republic.

[5]National Renewable Energy Lab, US Department of Energy

[*]Corresponding author: Colin P. Evans (cpe28@cornell.edu)

Key Points:

- A LIM is used to quantify the natural variability in the ENSO-SWUS teleconnection, and it suggests considerable intrinsic variability.
- This natural variability demonstrates that detecting anthropogenic changes in the ENSO-SWUS hydroclimate teleconnection will be difficult.
- CMIP6 shows an improvement in modeling the ENSO-SWUS teleconnection, but uncertainty remains in the projected future climate.

Abstract

Hydroclimate variability of the southwest United States (SWUS) is influenced by the tropical Pacific Ocean, particularly the phase of the El Niño/Southern Oscillation (ENSO), via teleconnections, which are expected to be altered by climate change. However, natural variability in this teleconnection has not been robustly quantified, complicating the detection of anthropogenic climate change. Here, we use a linear inverse model (LIM) to quantify natural variability in the ENSO-SWUS teleconnection. The LIM yields realistic teleconnection patterns with century-scale variability in teleconnection strength comparable to simulations from the Last Millennium Ensemble project and the Coupled Model Intercomparison Project Phases 5 and 6. The variability quantified by the LIM illuminates two aspects of our understanding of ENSO and its impacts: the inherent statistics of the observable system can produce century-long periods of nonsignificant correlation, and detecting changes in ENSO-related hydroclimate variability is challenging in a changing climate.

Plain Language Summary

The ENSO affects weather and climate across the globe through teleconnections. For example, when tropical Pacific Ocean sea surface temperatures (SSTs) are warmer than normal (e.g., during an El Niño), higher than normal amounts of rain are expected in the SWUS. However, we do not know how much natural variability there is in this teleconnection. That is, we do not know how often El Niños actually bring more rain to the SWUS. Because we have a relatively short history of observations, assessing this natural variability is difficult. Here, we use a statistical model to emulate the inherent statistics of ENSO teleconnections from observations. Doing so demonstrates that there is considerable intrinsic variability in the ENSO teleconnection to the SWUS. This suggests that even though ENSO and its effect on weather and climate are expected to change due to climate change, detecting such changes will be difficult.

1 Introduction

The El Niño/Southern Oscillation (ENSO) is the dominant source of interannual variability in the tropical Pacific Ocean with observable teleconnections to many parts of the globe. Despite the abundance of research into this phenomenon and its teleconnections, there are important aspects of ENSO that remain unknown. For instance, Yeh et al. (2018) examined general circulation models (GCMs) from both the Coupled Model Intercomparison Project Phases 3 and 5 (CMIP3 and CMIP5) and found that they do not yield a consistent picture of how ENSO and its teleconnections will change during the 21st century. While some studies have found consistent changes for a subset of these GCMs and the most extreme of ENSO events (Cai et al., 2018), others have identified a close relationship between mean state biases in these GCMs and their responses to anthropogenic climate change (Stevenson et al., 2021). Further analysis of GCMs showed how their cold bias in the Pacific cold tongue resulted in the inability to predict the recent cooling of the east Pacific (Seager et al., 2019).

Uncertainty in future projections of ENSO and its teleconnections present a critical outstanding problem, and yet there is still much left to be understood about ENSO in our current climate. This is also true for the simulation of ENSO by GCMs and the characteristics and physics of ENSO in the real world. The simulated strength and spatial pattern of ENSO teleconnections in our current climate varies considerably across GCMs (Langenbrunner & Neelin, 2013; Weare, 2013; Yeh et al., 2018). Likewise, it has been well established that the GCMs have biases in ENSO, which include too much SST variability, a weak annual cycle, and El Niños that propagate too far eastward from what is observed (Chen et al., 2017). Even when SST anomalies are nudged toward observations, composite ENSO events in an ensemble of GCMs showed considerable variability in teleconnection statistics (Deser et al., 2018).

Because of short observational records, we do not have a sufficient real-world baseline for natural variability in ENSO and its teleconnections. High resolution datasets of tropical Pacific sea surface temperatures (SSTs) are only available since 1948, which, using the operational definition of ENSO from the National Center for Environmental Prediction (NCEP), gives us only 11 observed El

Niño events and 6 or 7 observed La Niña events from which to draw conclusions (NCEP, 2019). While ENSO is the primary driver of interannual hydroclimate variability in the southwest US (SWUS, 32°N-40°N, 120°W-105°W, Fig. 1B), wherein El Niño (La Niña) brings anomalously high (low) amounts of rain to the region (Redmond and Koch, 1991, Cook et al., 2018), we lack a clear picture of the stability of this teleconnection. This is critical to understand because not only are the observed responses of ENSO on SWUS hydroclimate inconsistent between individual events, but different intensities of ENSO can also even change the sign of precipitation anomalies over the SWUS (Hoerling and Kumar, 2002). More recently, the 2015/16 El Niño, despite being one of the strongest in the observational record (Zhai et al., 2016), did not result in wetter conditions across the SWUS, and thus many areas of the region, especially Southern California, remained in severe drought conditions. The Pacific

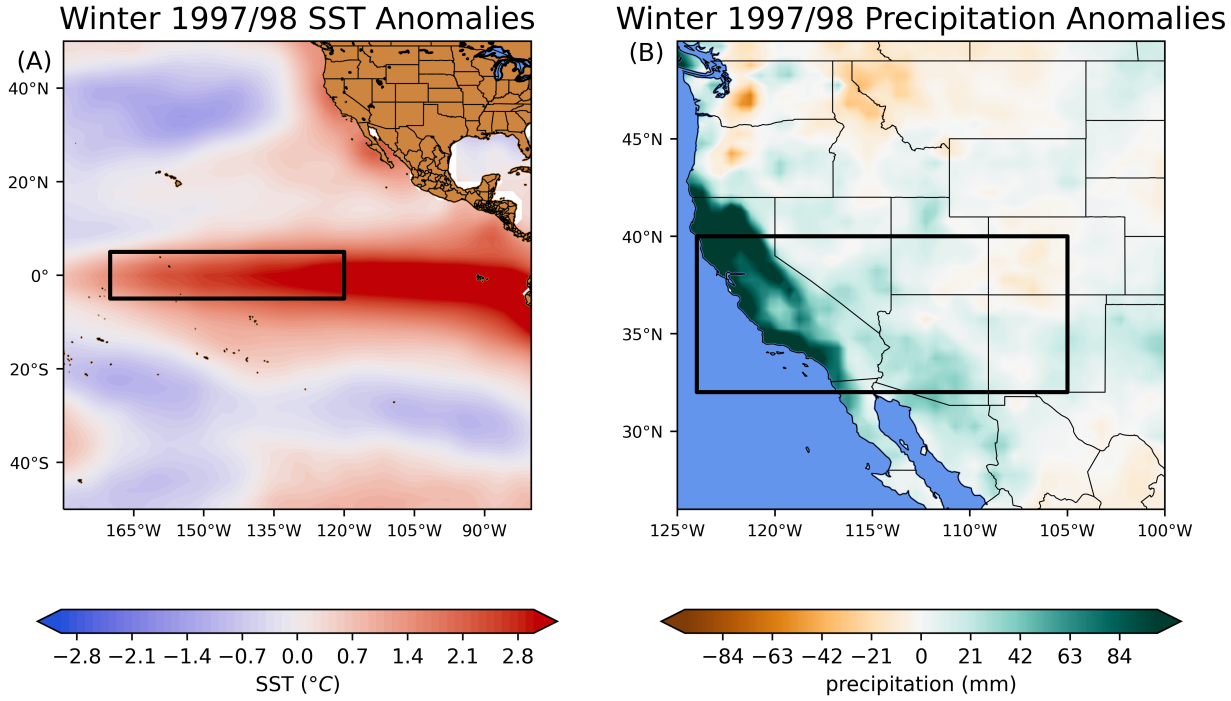

Figure 1 – A "typical" ENSO teleconnection to the SWUS, with (A) winter (DJF) SST anomalies against the 1951-1980 climatology using ERSSTv3b in the color contours, and the Niño3.4 region within the Pacific Ocean, covering 5°S-5°N and 170°W-120°W in the box, and (B) the southwestern United States with a box over the specific study area covering 32°N-40°N and 120°W-105°W, with precipitation anomalies against the 1951-1980 climatology using GPCC gridded data (Schneider et al., 2011) in the color contours.

Decadal Oscillation (PDO) can act as a modulating force on ENSO teleconnec-

tions, where a positive ENSO phase combined with a warm PDO is expected to increase the amount of rain brought to the SWUS (Wang et al., 2014). However, for the 2015/16 ENSO event, the PDO was in a warm phase, and yet the SWUS did not receive anomalous precipitation. The fact that the SWUS still did not experience wetter conditions then suggests that other internal atmospheric variability, or other modes of coupled atmosphere-ocean variability, can dominate hydroclimate variability in the SWUS. In support of an important role for internal atmospheric variability, Chen and Kumar (2018) analyzed ensemble forecasts for the 2015/16 winter season and found large differences in forecasted winter precipitation for the SWUS between ensemble members of the NCEP operational Climate Forecast System, version 2 (CFSv2).

Previous research into natural variability in ENSO teleconnections have largely used GCMs or relied on the limited observational record. For instance, Coats et al. (2013) found a high amount of time variability in ENSO teleconnection strength between winter (December-January-February--DJF) tropical Pacific SSTs and DJF 200-mb geopotential heights over North America in the control runs of CMIP5. In forced transient simulations from the same GCMs, a similar level of time variability in ENSO teleconnections was found (Lewis & LeGrande, 2015). However, results also showed that the spatial features of the teleconnections vary considerably across GCMs (Langenbrunner & Neelin, 2013; Coats et al., 2013), with implications for the real-world relevance of these results. Likewise, within observational record, it has been suggested that ENSO teleconnections vary in both space and time, although these results are limited to shorter timescales of variability (e.g., Hu & Feng, 2001; Rajagopalan et al., 2000; Cole & Cook, 1998; Gershunov & Barnett, 1998). Deser et al. (2018) showed that ENSO teleconnection strength can range more than twofold in certain locations.

Paleoclimate records can extend the observational record, and thus hold promise for characterizing natural variability in the ENSO teleconnection to the SWUS hydroclimate. For instance, using paleoclimate records, Ashcroft et al. (2016) found that real-world ENSO teleconnection to Australian precipitation varies through time. However, the quality of hydroclimate reconstructions in the SWUS are directly dependent on the number of tree-ring sites and the age of the trees (Cook et al., 2016), which decrease further back in time (Cook et al., 2016). Specifically, as the network of sites becomes sparser, reconstructions rely on sophisticated statistical techniques to fill in the missing data resulting in a loss of fidelity (Cook et al., 2016). Creating paleo records of tropical Pacific SSTs, specifically for the Niño3.4 region (5°S-5°N, and 170°W-120°W, Fig. 1A), is even more difficult. There are few coral reefs in the region, and so creating in situ reconstructions for the region is largely not possible (Cobb et al., 2003, Emile-Geay et al., 2017). Any SST reconstructions for the Niño3.4 region are instead derived from sites covering a large spatial range and then extrapolated for the region, resulting in significant uncertainties (Emile-Geay et al., 2017).

To address the limitations of the short observational record, the uncertainty

in paleoclimate records, and the biases inherent to GCMs, we used a Linear Inverse Model (LIM) to characterize variations in the ENSO teleconnection to the SWUS hydroclimate (ENSO-SWUS teleconnection) that are inherent to the observational record. That is to say, what range of ENSO-SWUS teleconnection characteristics is expected given the statistics of observations? We also use the LIM to benchmark observations and global climate model (GCM) ensembles from the Last Millennium Ensemble (LME), CMIP5, and CMIP6.

A LIM offers an empirical approach to emulating the statistics of an observable system. Importantly, we can do so with observation datasets of high quality, i.e., high temporal and spatial resolution, thus minimizing sources of uncertainty. LIMs have been applied to examine and determine the significance of low frequency variability in the tropical Pacific on decadal timescales (Ault et al., 2013), the significance of "Modoki" El Niño events (Newman et al., 2011), determine the predictability of the Pacific Decadal Oscillation (Newman et al., 2016), and to test the significance of tropical Pacific SST gradient trends relative to internal variability (Coats and Karnauskas, 2017). Other studies have utilized a LIM to make seasonal ENSO predictions (Penland and Sardeshmukh, 1995), and to evaluate the ability of GCMs to make decadal forecasts (Newman, 2013). Additionally, the LIM has been shown to successfully reproduce ENSO and PDO statistics and can outperform certain forecast models (Perkins and Hakim, 2019) and it has been used to predict Pacific SST anomalies (Alexander, et al., 2008). The LIM, thus, is a perfect tool with which to create benchmark for the ENSO-SWUS hydroclimate variability.

2 Data and Methodology

2.1 Constructing the LIM

Herein we build upon the LIM used by Penland and Matrsosova (1994) and Penland and Sardeshmukh (1995), and more recently that of Ault et al. (2018) and Coats et al. (2020), with some specific changes to its construction. First, SST anomalies were calculated using the National Ocean and Atmospheric Administration (NOAA) Extended Reconstructed Sea Surface Temperature V3b (ERSSTV3b; Smith et al., 2008), which is a monthly dataset of SSTs spanning 1854 to present on a 2° latitudinal by longitudinal grid. For the SWUS, reconstructions of the Palmer Drought Severity Index (PDSI) are an often-used proxy for drought conditions. The observational PDSI input data used was created by Sheffield et al. (2006) and is a 1° resolution monthly dataset spanning 1948-2008. Second, to isolate the ENSO and SWUS hydroclimate teleconnection, we restricted the domain of the SST anomalies to that of just the Niño3.4 region and restricted the PDSI to the SWUS.

Auto-regressive models can be used to examine the significance of single-variable scalar time series. The LIM (Eq. 1) is analogous to an AR(1) process, but adapted for the multivariate setting (Penland & Sardeshmukh, 1995). The linear deterministic feedback matrix (L) in Equation 1, calculated using Equation 2, provides information on how random perturbations propagate forward through

time in a state variable, such as X**,** which in this case is PDSI and SST anomalies. is the white-noise forcing term used to perturb the system (Penland and Sardeshmukh, 1995).

$$\frac{\mathrm{dX}}{\mathrm{dt}} = LX + \zeta \quad (1)$$

$$L = \ n^{-1} \ln \ln \ \left(\frac{C_n}{C_o}\right) \quad (2)$$

The linear deterministic feedback matrix is calculated from empirical data, where C_n is the lag covariance matrix at time lag n, C_o is the instantaneous covariance matrix, and n is the time lag parameter. For our purposes, the time lag is set to 3 months to account for the seasonality, though changes in this parameter do not consequently change the value of L (Ault et al., 2018).

The important assumption of the LIM is that the system being modeled is linear, which is not the case for the real climate system. However, through smoothing and averaging, the nonlinear system yields a system of state vectors that are approximately Gaussian (Yuval and Hsieh, 2002). Penland and Sardeshmukh (1995) and Newman (2013) have both shown the validity of this approach using monthly SST anomalies.

As in Ault et al. (2018), we aimed for our LIM to meet the following criteria: (a) it captured the observed correlation pattern between SWUS PDSI and Niño3.4 region SST anomalies; (b) it reproduced realistic variance in SWUS PDSI and Niño3.4 region SST anomalies; and (c) it generated the 2–7-year peak in variability of ENSO events in the Niño3.4 region. We ran the LIM for 100,000 years to provide a population of 1,000 100-year periods. From there we computed the century-scale correlation values between SWUS PDSI and Niño3.4 SST anomalies for each 100-year period, to produce a range of 1000 correlation values.

2.2 PDSI from Models

As in Ault et al. (2018) we used PDSI to characterize the hydroclimate of the SWUS, which we calculated offline using available variables from CMIP5, CMIP6, and LME. Following the work by Herrera & Ault (2017) we used the self-calibrating version of the PDSI (Eq. 3), with the FAO Penman-Monteith method (Penman, 1948; Monteith, 1965) for calculating potential evapotranspiration (Eq. 4; e.g., Smerdon et al., 2015). This FAO method is based on the original Penman-Monteith equation but instead uses fewer variables and assumes an ideal grass surface with specific parameters (i.e., a constant water supply, Allen et al., 1998)

$$X_i = \ \mathrm{pX}_{i-1} + \mathrm{qZ}_i \ (3)$$

$$PET = \ \frac{0.408\,(Rn-G) + \ \gamma \frac{900}{T+273.16} U_2 (e_s - e_a)}{+ \ \gamma(1+0.34U_2)} \ (4)$$

For equation 3, X_i is the PDSI value for a specific month, $X_{i\text{-}1}$, is the PDSI from the previous month at that location, p and q are autocorrelation duration

factors, and Z_i is the current moisture anomaly. Table 1 details the variables and units for the PET equation.

2.3 Model Analyses

We used 9 runs of the forced transient LME experiments, each spanning 850-1950, and calculated century-length correlations for the ENSO-SWUS teleconnection for a total of 99 correlation values. For CMIP5 and CMIP6 we calculated the teleconnection strength (Pearson correlation) in the historical experiments to determine if there have been improvements in the simulation of ENSO-SWUS teleconnections in the new generation of GCMs, and to provide a baseline for the analysis of future projections. For CMIP6, we also calculated the future teleconnection strength (2015-2100) using the Shared Socioeconomic Pathway 5-8.5 (SSP585, O'Neill, et al., 2016) emissions scenario, to quantify changes to ENSO -SWUS teleconnections due to climate change. A total of 15 GCMs from CMIP5 (Table 2) and 11 GCMs from CMIP6 (Table 3) had the requisite variables needed to calculate PET.

Table 1. The variables, description, and units of the PET equation (S4).

Variable	**Description**	**Units**
Rn	net radiation	MJ $m^{-2}day^{-1}$
G	soil heat flux density	MJ $m^{-2}day^{-1}$
T	2-meter temperature	°C
γ	psychrometric constant	kPa $°C^{-1}$
U_2	2-meter wind speed	ms^{-1}
e_s-e_a	vapor pressure deficit	kPa
	slope of the vapor pressure curve	kPa $°C^{-1}$

Table 2: CMIP5 ensemble model information

Modeling Center
Canadian Centre for Climate Modelling Analysis
National Center for Atmospheric Research
Center National de Recherches Météorologiques/Centre de Recherche et Formation Avancée Calcul Scientifiqu
Commonwealth Scientific and Industrial Research Organization in collaboration with Queensland Climate Ch
NOAA Geophysical Fluid Dynamics Laboratory
NASA Goddard Institute for Space Studies
Institute for Numerical Mathematics
Institute Pierre-Simon Laplace
Japan Agency for Marine-Earth Science and Technology, Atmosphere and Ocean Research Institute (The Uni
Meteorological Research Institute
Norwegian Climate Centre

Table 3: CMIP6 ensemble model information

Modeling Center
Commonwealth Scientific and Industrial Research Organization
Beijing Climate Center
National Center for Atmospheric Research
Canadian Centre for Climate Modelling and Analysis
NOAA Geophysical Fluid Dynamics Laboratory
Institute Pierre-Simon Laplace
Japan Agency for Marine-Earth Science and Technology, Atmosphere and Ocean Research Institute (The Uni
Deutsches Klimarechenzentrum
Meteorological Research Institute

3 Results

3.1 Validation of LIM framework

Previous LIM studies used principal component (PC) analysis to reduce the dimensionality of each variable, and a 3-month running average was used to smooth each time series prior to computing the PCs (Ault, et al., 2018). As such, a limitation of the LIM is that it cannot reproduce 100% of the variance in the system. For SSTs, the first 27 PCs accounted for 94.9 percent of the total variance. For PDSI, 20 PCs were retained for 95.1 percent of the variance. Additionally, the LIM output met all of the validation criteria: it captured the observed correlation pattern between SWUS PDSI and Niño3.4 region SST anomalies (Fig. 2), it reproduced realistic variance in SWUS PDSI and Niño3.4 region SST anomalies, and it generated the 2–7-year variability of ENSO events in the Niño3.4 region (Fig. 3). The modeled ENSO-SWUS teleconnection is very similar to that of the observational dataset (Fig. 2). While the construction of the LIM prevents 100% of the variance being retained, the LIM does reproduce the realistic variance found in the observations. Lastly, the LIM can capture both the low-frequency and high-frequency variability in tropical Pacific SST anomalies (Fig. 3).

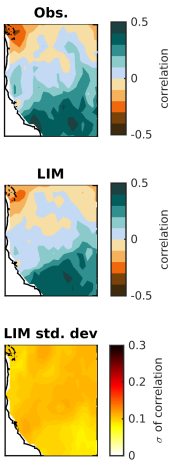

Figure 2 – The observed correlation pattern between Niño3.4 SSTs and SWUS PDSI (top) and the modeled correlation pattern from the LIM (bottom).

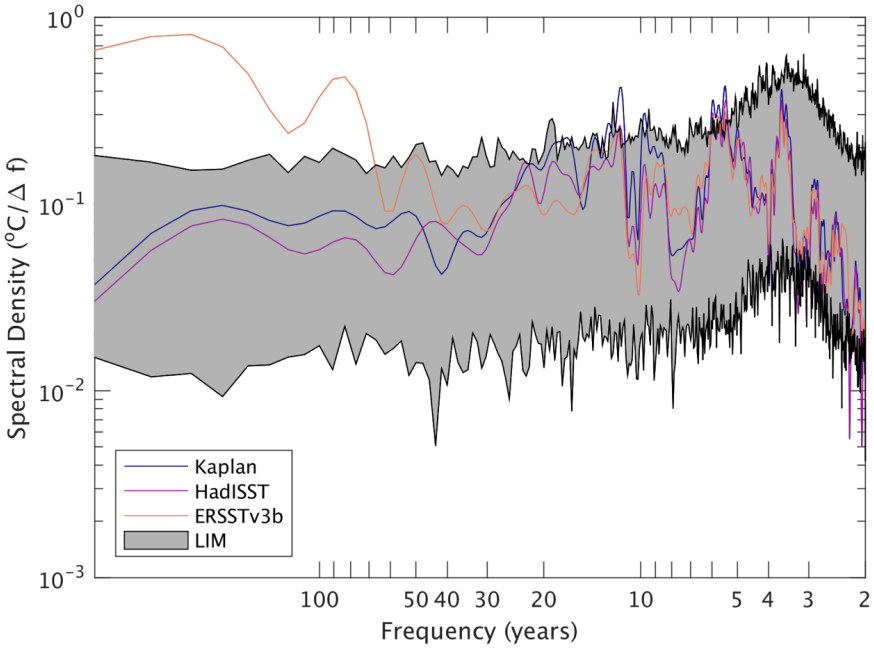

Figure 3 – The power spectrum of Niño3.4 observational time series (colored lines) and for the ensemble of LIM realization (grey shading). The LIM ensemble largely captures the low and high-frequency variability of the tropical Pacific SSTs.

3.2 Internal Variability in the LIM

We first assessed the inherent variability in the ENSO-SWUS teleconnection strength by quantifying the range of possible correlations between Niño3.4 SSTs and SWUS PDSI that are consistent with the inherent statistics of the observational dataset as sampled by the LIM. The LIM simulated a broad empirical distribution (Fig. 4), suggesting that considerable natural variability can emerge intrinsically, even from the relatively stable and short climatic interval sampled by the observational datasets. More than 70% of the correlations calculated fell between 0.3 and 0.6, while over 90% fell between 0.2 and 0.6 (Fig. 4) The ensemble mean correlation from the LIM was 0.35, compared to a correlation of 0.37 calculated from the observational dataset.

3.3 Internal Variability in the GCMs

The LME correlation values show a smaller range in teleconnection strength than the LIM, with correlations ranging from 0.45 to 0.75 (Fig. 5). This narrower range is found despite the LME simulating the entire last millennium, and thus also simulating external forcings and long timescale internal variability not sampled by the LIM. Importantly, the ensemble mean correlation from the LME of 0.65 is much greater than that from the LIM, consistent with previous research suggesting that CESM1 (the GCM used in the LME) has an overly strong ENSO-SWUS teleconnection (e.g., DiNezio et al, 2017). The range of correlations from the LME is narrower than that from the CMIP5 or CMIP6 simulations (Fig. 6 and below), suggesting that inter-GCM structural differences in ENSO-SWUS teleconnection strength are larger than the natural variability in this metric as simulated by a single GCM. The ensemble mean correlation from the LME is also higher than that of the CMIP5 or CMIP6 ensembles, and thus overly strong ENSO-SWUS teleconnections are not a general feature of GCMs.

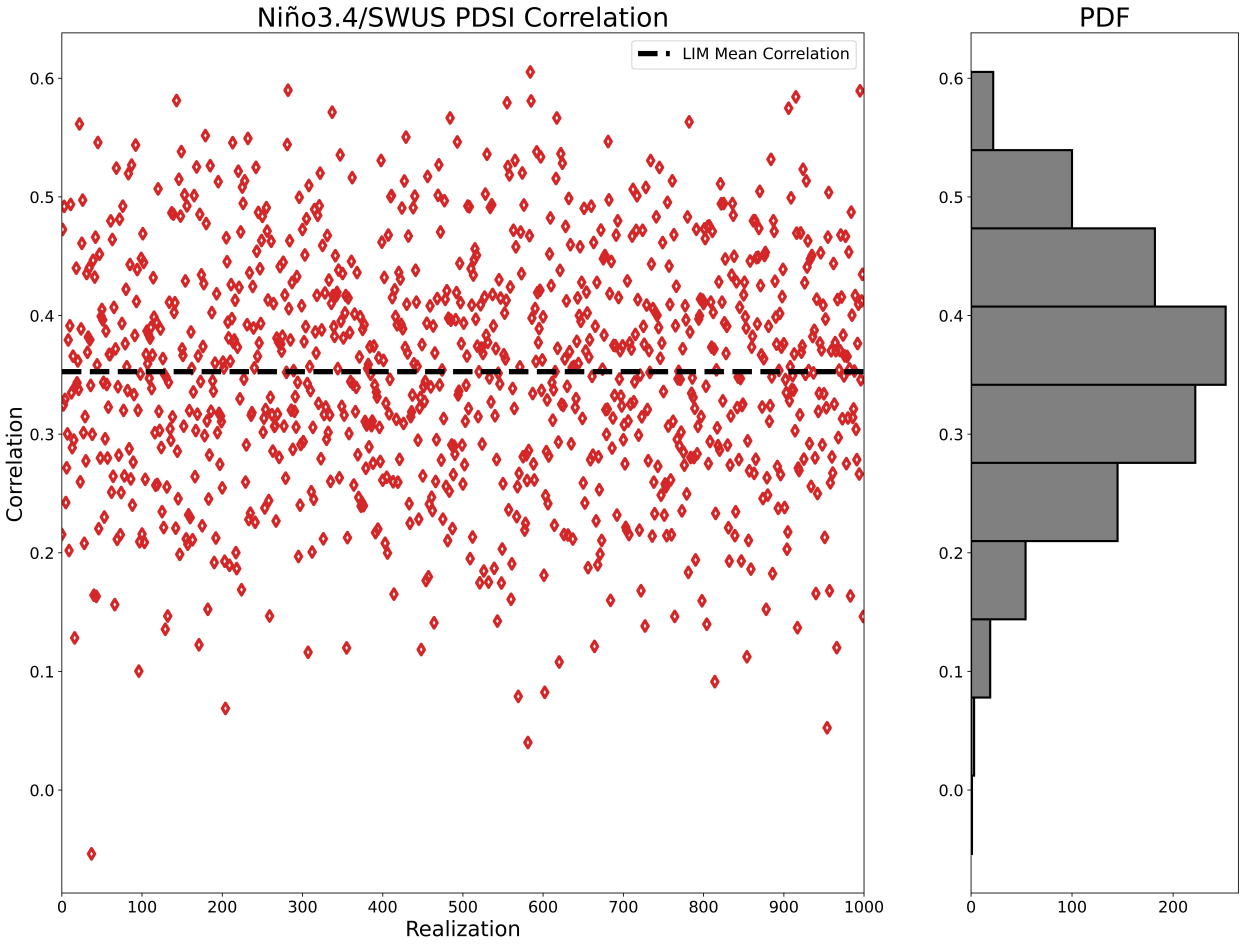

Figure 4 – The 1000 century-long correlation values calculated from the LIM generated Niño3.4 SSTs and SWUS PDSI. On the right, an empirical distribution for all 1000 century-long correlation values. The red dotted line is the ensemble mean for all 1000 century-long correlation values.

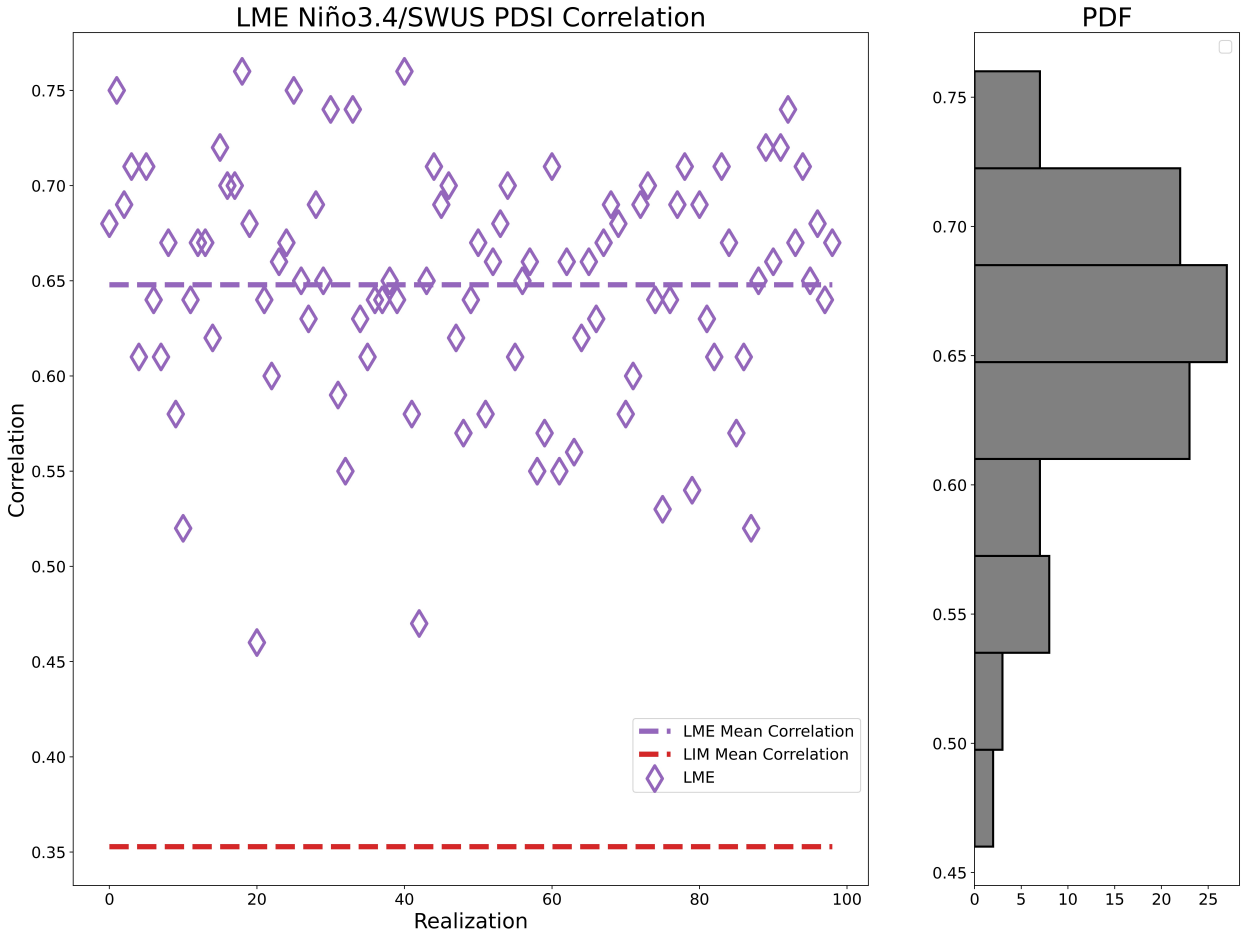

Figure 5 – Correlation values between Niño3.4 SSTs and SWUS PDSI calculated from 99 distinct century-long periods from the LME (Methods), with an empirical distribution in the panel to the right. The purple dotted line is the ensemble mean correlation value from the LME and red dotted line is the ensemble mean from the LIM.

In the CMIP5 simulations, ENSO-SWUS teleconnections vary in strength, and even in sign, across the GCMs. For instance, CNRM-CM5 exhibits a negative correlation between Niño3.4 SSTs and SWUS PDSI, whereas GFDL-ESM2M exhibits a correlation of over 0.8 (Fig. 6). Although the ensemble mean correlation of the CMIP5 simulations was close to that from the LIM, the range is much wider (Fig. 6) and the distribution more uniform (Fig. 8). Of relevance to the ability of CMIP5 GCMs to simulate ENSO-SWUS teleconnection strength, there are 4 GCMs with correlations below 0.2 (the bottom of the LIM range), indicating too weak of a relationship between Niño3.4 SSTs and SWUS PDSI. Likewise, there are five GCMs with correlations higher than 0.6 (the top of the

LIM range), indicating an overemphasis of this relationship.

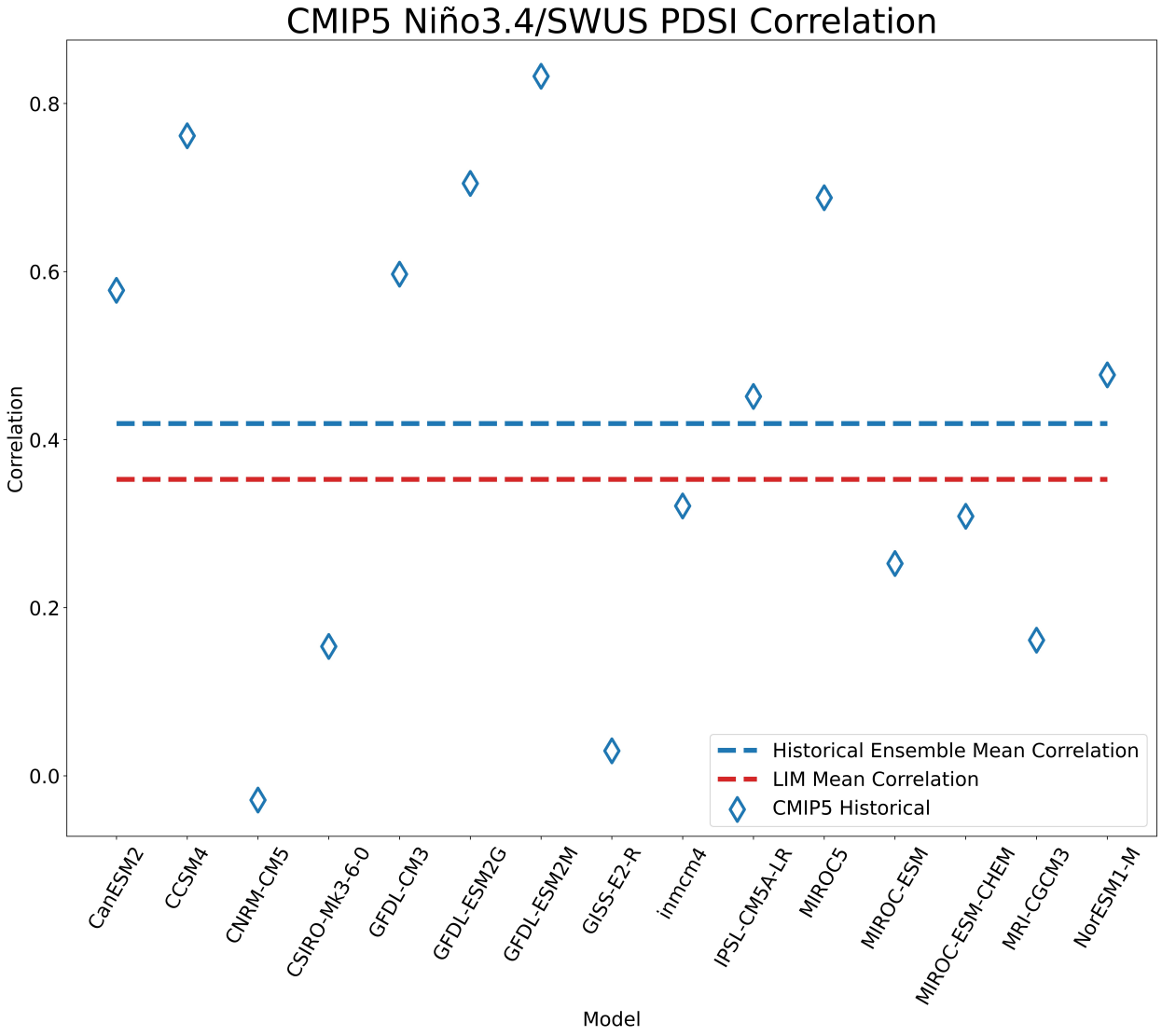

Figure 6 – Calculated correlation values between Niño3.4 SSTs and SWUS PDSI from the CMIP5 historical simulations. Blue dotted line is the ensemble mean correlation value from the CMIP5 simulations and the red dotted line is the ensemble mean from the LIM.

Overall, the CMIP6 simulations exhibit ENSO-SWUS teleconnection strengths that are more consistent with the LIM as compared to the previous generation of GCMs (Fig. 7). The ensemble mean correlation of 0.3 for the CMIP6 simulations is closer to the ensemble mean of the LIM (0.35) than the CMIP5

simulations (0.42), and the distribution is narrower and more consistent with the LIM, with a range of about 0.1 to 0.5 for CMIP6 as compared to about 0 to 0.8 for CMIP5. There are large changes in teleconnection strength from CMIP5 to CMIP6 for individual modelling centers. For instance, the correlation from GFDL-ESM4 (CMIP6) is a more realistic 0.3 (within the LIM range), as compared to the average correlation of 0.71 from the 3 GFDL GCMs from CMIP5. Likewise, while the NCAR GCMs CESM1 (LME – Fig. 5) and CCSM4 (CMIP5 – Fig. 6) exhibited correlations largely in excess of the LIM, CESM2 (CMIP6 – Fig. 7) exhibits a correlation that is below the LIM range (Fig. 7). Importantly, we also find an improvement in capturing the ENSO-SWUS teleconnection in CMIP6 from modeling centers with members in both CMIP5 and CMIP6 (not shown) as well as an overall improvement in an ensemble of CMIP6 models (Fig. 8).

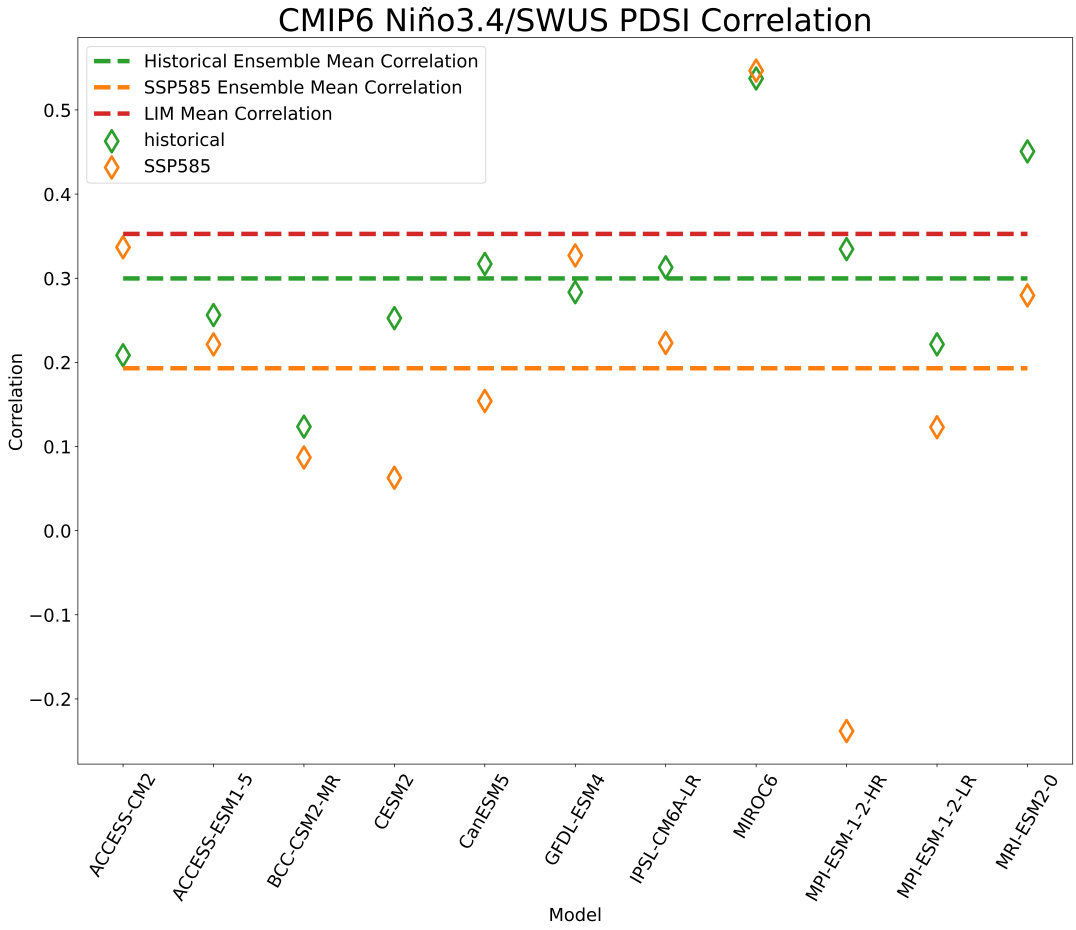

Figure 7 – Calculated correlation values between Niño3.4 SSTs and SWUS PDSI calculated from the CMIP6 simulations for both the historical (green) experi-

ments and future experiments (SSP585 - orange). The red dotted line is the ensemble mean from the LIM.

Finally, to assess if there are consistent changes in the ENSO-SWUS teleconnection strength in the future, we also analyzed data from the CMIP6 SSP585 simulations, which are run with a high emissions scenario and thus should exhibit a large signal (climate change) to noise (natural variability) ratio. Eight of the 11 GCMs exhibit a decrease in the ENSO-SWUS teleconnection strength in the 21^{st} as compared to the 20^{th} centuries (Fig. 7), with a change in the ensemble mean correlation from 0.3 to 0.2, respectively. Together, the CMIP6 simulations thus suggest a small but significant decrease in ENSO-SWUS teleconnection strength in the future. To summarize, Figure 8 illustrates the ENSO-SWUS teleconnection strength and variability in each of the analyzed ensembles.

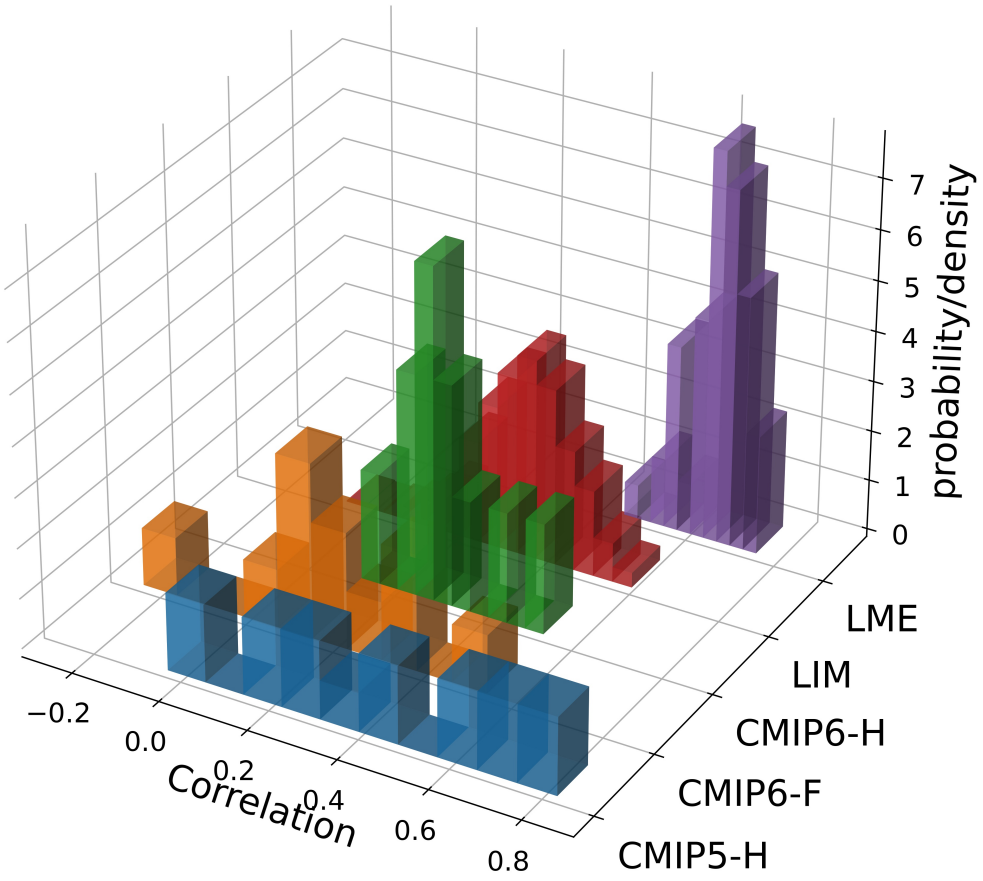

Figure 8 – Density/probability plot comparison of ENSO-SWUS teleconnection strength for the historical run of CMIP5 (blue), CMIP6-SSP585 (orange), CMIP6-Historical (green), LIM (red), and the LME (purple).

4 Discussion

We used a LIM to quantify the intrinsic natural variability in ENSO-SWUS teleconnections that is expected intrinsically – i.e., the range of teleconnection strength possible given the inherent statistics of an observational dataset. We found that the LIM accurately captures the ENSO variability, and spatial and temporal ENSO-SWUS correlation patterns found in the observational dataset. It also exhibits considerable variability in the ENSO-SWUS teleconnection strength. Most importantly, our results exhibit entire centuries of non-

significant correlation (roughly 3-6% of the centuries in the LIM). The LIM does not possess long-term sources of variability, as the output drawn from the LIM relies solely on the 3-month time-lag parameter, calculated from the inherent statistics of the observational dataset. Because of this, the LIM samples only a narrow range of plausible behaviors of the system, effectively removing any source of long-term internal or external forcing. Therefore, the LIM demonstrates that, for purely statistical reasons, Niño3.4 SSTs and SWUS PDSI correlations can be insignificant over a given century. This further indicates that it was not unreasonable to expect ENSO to have had no statistically significant impact on SWUS hydroclimate during the 20^{th} century, like in the results found by Ault et al. (2018). Finally, it is also reasonable to expect a diminished correlation in the future, even without climate change.

The ensemble mean correlation from the LIM was slightly lower than the observational dataset on which it was based (0.35 for the LIM compared to 0.37 from observations). While superficially interesting, this was an expected result given that the LIM does not retain 100% of the variance in the Niño3.4 SSTs and the SWUS PDSI (by retaining only the first few principal components of each). Within the timeframe of the observational dataset (1948-2008), there have been 7 strong El Niño events. Anomalously high PDSI in the SWUS was recorded only after 3 of these events (e.g., 1982-1983, 1988-1989, 1997-1998). Therefore, observations alone indicate that not all ENSO events affect SWUS hydroclimate. Results from the LIM strengthen this conclusion, demonstrating that intrinsic variability is a robust feature of the ENSO-SWUS teleconnection.

In the LME, the ENSO-SWUS teleconnection is much stronger than in observations or the LIM, placing more importance on ENSO for driving SWUS hydroclimate than is realistic. This undoubtedly undermines our confidence in the ability of CESM1 to accurately project the response of this teleconnection to external forcing, and specifically climate change. This study provides further evidence that tools like the LIM that can be used to assess the ability of GCMs to simulate coupled atmosphere-ocean dynamics and can provide an important benchmark as we continue to use GCMs to project climate change.

With such benchmarking in mind, the ensemble mean correlations are similar between the LIM, CMIP5, and CMIP6. Nevertheless, it is also important to focus on the distribution of these correlations. Our results with the GCMs are consistent with previous studies that found large variability in ENSO teleconnection strengths between GCMs (e.g. Coats et al., 2013; Cook et al., 2016). While there is evidence for improvement in the teleconnection strength in the CMIP6 GCMs, we find that there is still a wide range in their ability to simulate ENSO-SWUS teleconnections. Further analysis, particularly on a process level, and of the outliers in correlation in the CMIP5 and CMIP6 ensembles could lend insight into the physical processes most important to realistically simulating ENSO-SWUS teleconnection. Nevertheless, to robustly determine which of these GCMs best represents the statistics of the real world will require ensembles of each, like the LME, such that the true distribution of correlations can

be quantified. In the absence of such ensembles, training LIMs on the GCMs themselves may be a useful, though imperfect, path forward (e.g., Coats et al., 2020)

Drought remains an obstacle for water resource managers in the SWUS. Uncertainty in the strength of ENSO-SWUS teleconnections further complicates water resource management. Despite the advances in computational power and forecast modeling, the predictability of ENSO beyond the spring predictability barrier has not improved (Chen et al., 2020). This, when combined with the findings presented here, suggest that SWUS hydroclimate is largely unpredictable from year-to-year. Lack of predictability is particularly problematic when considering that it has been established that the lack of water resources has caused the collapse of several civilizations in the SWUS (Benson et al., 2002; Stahle & Dean, 2011). Furthermore, projections exhibit large declines in Colorado River flow in the coming decades (Udall & Overpeck, 2017), which is the main source of water for roughly 60 million Americans in the SWUS.

The results from our analysis of CMIP6 indicate that the ENSO-SWUS teleconnection has the potential to decrease in strength, both through intrinsic variability and in response to climate change. This leads to new questions, such as, if intrinsic variability and climate change decrease the strength of the ENSO-SWUS teleconnection, what fills this void? Studies have pointed towards the potential for a stronger land-atmosphere coupling effect. Although the SWUS is a largely soil-moisture limited environment, like the Great Plains (the land-atmosphere coupling "hot spot"), land-atmosphere coupling is not as strong in the SWUS, potentially due to the strength of the ENSO teleconnection (Koster et al., 2004; Santanello et al., 2018). As suggested in Dirmeyer et al. (2012), a weakening of the teleconnection could lead to a strengthening of land-atmosphere coupling, and this presents another interesting area for further analysis. Building a historical baseline like we have done here can help disentangle these different forcings, like local feedbacks and large-scale circulation patterns and teleconnections, and shed light on what to expect in a changing climate. Altogether, decreased teleconnection strength, intrinsic variability, and changing land-atmosphere interactions could mean fewer opportunities for the SWUS to replenish its water stores during El Niños, with potentially dire consequences for stakeholders in the region.

Acknowledgments and Data

The authors wish to thank the Emergent Climate Risk Lab at Cornell University for all the support and Dr. Adam Young for his insight and editing skills. Data for the CMIP models are available via the World Climate Research Programme, LME data is available from the National Center for Atmospheric Research, SST data is available from the National Ocean and Atmospheric Administration, and the observational PDSI data is available via the Terrestrial Hydrology Research Group at Princeton University. The output data from the LIM, and the PDSI data created from the LME, CMIP5, and CMIP6 are available through Cornell University eCommons (for publishing: https://doi.org/10.7298/8d7j-wt40).

This work was made possible through funding from the National Science Foundation awards AGS1751535 and AGS1602564.

References

Alexander, M.A., Matrosova, L., Penland, C., Scott, J.D., and Chang, P. (2008). Forecasting Pacific SSTs: Linear inverse modeling prediction of the PDO. *Journal of Climate, 21*(2), 385-402.

Allen, R., & Coauthors, (1998). Crop evapotranspiration: Guidelines for computing crop water requirements. *FAO Irrigation and Drainage Paper 56*, 300 pp.

Ashcroft, L., Gergis, J. & Karoly, D.J. (2016). Long-term stationarity of El Niño–Southern Oscillation teleconnections in southeastern Australia. *Climate dynamics, 46*(9-10), 2991-3006.

Ault, T., Deser, C., Newman, J., & Emile-Geay, J. (2013). Characterizing decadal to centennial variability in the equatorial Pacific during the last millennium, *Geophysical Research Letters, 40(13), 3450-3456.*

Ault, T., George, S., Smerdon, J., et al. (2018). A robust null hypothesis for the potential causes of megadrought in western North America, *Journal of Climate, 31, 3-24.*

Benson, et al. (2002). Holocene multidecadal and multicentennial droughts affecting Northern California and Nevada, *Quaternary Science Reviews, 21*(4-6), 659-682.

Cai, W., Wang, G., Dewitte, B., Wu, L., Santoso, A., Takahashi, K., Yang, Y., Carréric, A. & McPhaden, M.J. (2018). Increased variability of eastern Pacific El Niño under greenhouse warming. *Nature, 564*(7735), 201-206.

Chen, C., Cane, M.A., Wittenberg, A.T., & Chen, D. (2017). ENSO in the CMIP5 simulations: Life cycles, diversity, and responses to climate change, *Journal of Climate, 30*(2), 775-801.

Chen, H., Tseng, Y., Hu, Z., & Ding, R. (2020). Enhancing the ENSO predictability beyond the spring barrier, *Scientific Reports, 10*(984), 12pp.

Chen, M., and Kumar, A. (2018). Winter 2015/16 atmospheric and precipitation anomalies over North America: El Niño response and the role of noise, *Monthly Weather Review 146*(3), 909-927.

Coats, S. & Karnauskas, K.B. (2017). Are simulated and observed twentieth century tropical Pacific sea surface temperature trends significant relative to internal variability?, *Geophysical Research Letters, 44*(19), 9928-9937.

Coats, S., Smerdon, J., Cook, B., & Seager, R. (2013). Stationarity of the tropical Pacific teleconnections to North America in CMIP5/PMIP3 model simulations, *Geophysical Research Letters, 40*(18), 4927-4932.

Coats, S., Smerdon, J.E., Stevenson, S., Fasullo, J.T., Otto-Bliesner, B., & Ault, T.R. (2020). Paleoclimate constraints on the spatiotemporal character of past and future droughts, *Journal of Climate, 33*(22), 9883-9903.

Cole, J.E. & Cook, E.R. (1998). The changing relationship between ENSO variability and moisture balance in the continental United States, *Geophysical Research Letters, 25*(24), 4529-4532.

Cook, B., Cook, E., Smerdon, J., Seager, R., Williams, A., Coats, S., Stahle D., & Diaz, J. (2016). North American megadroughts in the Common Era: reconstructions and simulations, *WIRES: Climate Change, 7*(3), 411-432.

Cook, B., Williams, A., Mankin, J., et al. (2018), Revisiting the leading drivers of Pacific coastal drought variability in the contiguous United States, *Journal of Climate 31(1), 25-43.*

Deser, C., Simpson, I., Phillips, A., and McKinnon, K. (2018). How well do we know ENSO's climate impacts over North America, and how do we evaluate model accordingly? *Journal of Climate 31*(13), 4991-5014.

DiNezio, P.N., Deser, C., Karspeck, A., Yeager, S., Okumura, Y., Danabasoglu, G., Rosenbloom, N., Caron, J., and Meehl, G.A. (2017). A 2-year forecast for a 60-80% chance of La Niña in 2017-2018. *Geophysical Research Letters, 44*, 11,624-11,635.

Dirmeyer, P.A., Cash, B.A., Kinter III, J.L., Stan, C., Jung, T. et al. (2012). Evidence for enhanced land-atmosphere feedback in a warming climate. *Journal of Hydrometeorology, 13*(3), 981-995.

Gershunov, A. & Barnett, T. (1998). Interdecadal modulation of ENSO teleconnections, *Bulletin of the American Meteorological Society, 79*(12), 2715-2725.

Herrera, D. & Ault, T. (2017). Insights from a new high-resolution drought atlas for the Caribbean spanning 1950-2016, *Journal of Climate, 30*(19), 7801-7825.

Hoerling, M.P. and Kumar, A. (2002). Atmospheric response patterns associated with tropical forcing. *Journal of Climate, 15*(16), 2184-2203.

Hu, Q. & Feng, S. (2001). Variations of teleconnections of ENSO and interannual variation in summer rainfall in the central United States, *Journal of Climate, 14*(11), 2469-2480.

Koster, R.D., Dirmeyer, P.A., Guo, Z., Bonan, G. et al. (2004). Regions of strong coupling between soil moisture and precipitation. *Science, 305*(5687), 1138-1140.

Langenbrunner, B. & Neelin, J. (2013). Analyzing ENSO teleconnections in CMIP models as a measure of model fidelity in simulating precipitation, *Journal of Climate, 23(13),* 4431-4446.

Lewis, S.C. & LeGrande, A.N. (2015). Stability of ENSO and its tropical Pacific

teleconnections over the Last Millennium. *Climate of the Past, 11*(10), 1347-1360.

Monteith, J. L., (1965). Evaporation and environment. *19th Symp. of the Society for Experimental Biology*, Swansea, England, Society for Experimental Biology, 205–234.

NCEP (2019). El Niño Index Dashboard, Niño3.4 Time Series, retrieved from esrl.noaa.gov.

Newman, M., Alexander, M., & Scott, J. (2011). An empirical model of tropical ocean dynamics, *Climate Dynamics, 37(9-10), 1823-1841.*

Newman, M. (2013). An empirical benchmark for decadal forecasts of global surface temperature anomalies, *Journal of Climate, 26*, 5260-5269.

Newman, M., Alexander, M., Ault, T., et al. (2016). The Pacific decadal oscillation, revisited, *Journal of Climate, 29(12), 4399-4427.*

O'Neill, B.C., Tebaldi, C., van Vuuren, D.P., Eyring, V., Friendlingstein, P., Hurtt, G., et al. (2016). The scenario model intercomparison project (scenario MIP) for CMIP6, *Geosciences Model Development, 9,* 3461-3482.

Penland, C. & Matrosova, L. (1994). A balance condition for stochastic numerical models with application to the El Niño-Southern Oscillation, *Journal of Climate, 7*(9), 1352-1372.

Penland, C. & Sardeshmukh, P. (1995). The optimal growth of tropical sea surface temperature anomalies, *Journal of Climate, 8*(8), 1999-2024.

Penman, H.L. (1948). Natural evaporation from open water, bare soil and grass, *Proc. Roy. Soc. London, 193*, 120-145.

Perkins, W.A. and Hakim, G.J. (2020). Linear inverse modeling for coupled atmosphere-ocean ensemble climate prediction. *Journal of Advances in Modelling Earth Systems 12*(1), 15 pp.

Rajagopalan, B., Cook, E., Lall, U., & Ray, B.K. (2000). Spatiotemporal variability of ENSO and SST teleconnections to summer drought over the United States during the twentieth century, *Journal of Climate, 13*(24), 4244-4255.

Redmond, K. and Koch, R. (1991), Surface climate and streamflow variability in the Western United States and their relationship to large-scale circulation indices, *Water Resources Research, 27*(9), 2381-2399.

Santanello, J.A., Dirmeyer, P.A., Ferguson, C.R., Findell, K.L., Tawfik, A.B. et al. (2018). Land-atmosphere coupling interactions: The LoCo perspective. *Bulletin of the American Meteorological Society, 99*(6), 1253-1272.

Schneider, U., Becker, A., Finger, P., Meyer-Christoffer, A., Rudolf, B., and Ziese, M. (2011) GPCC Full Data Reanalysis Version 6.0 at 0.5°: monthly land-surface precipitation from rain-gauges built on GTS-based and historic data. doi: 10.5676/DWD_GPCC/FD_M_V6_050

Seager, R., Cane, M., Henderson, N., Lee, D., Abernathy, R., and Zhang, H. (2019). Strengthening tropical Pacific zonal sea surface temperature gradient consistent with rising greenhouse gases. *Nature Climate Change, 9,* 517-522.

Sheffield, J., G. Goteti, & Wood, E.F. (2006). Development of a 50-yr high-resolution global dataset of meteorological forcings for land surface modeling, *Journal of Climate, 19(13),* 3088-3111.

Smerdon, J. E. Cook, B. I., Cook, E. R. & Seager, R. (2015). Bridging past and future climate across paleoclimatic reconstructions, observations, and models: A hydroclimate case study, *Journal of Climate, 28*, 3212–3231.

Smith, T.M., Reynolds, R.W., Peterson, T.C., & Lawrimore, J. (2008). Improvements to NOAAs historical merged land–ocean surface temperature analysis (1880–2006), *Journal of Climate, 21*, 2283–2296.

Stahle, D. & Dean, J. (2011). North American tree rings, climatic extremes, and social disasters, *Dendroclimatology, 11*, 297-327.

Stevenson, S., Wittenberg, A.T., Fasullo, J., Coats, S. & Otto-Bliesner, B. (2021). Understanding Diverse Model Projections of Future Extreme El Niño, *Journal of Climate, 34*(2), 449-464.

Udall, B. & Overpeck, J. (2017). The twenty-first century Colorado River hot drought and implications for the future, *Water Resources Research, 53*(3), 2404-2418.

Wang, S., Huang, J., He, Y., and Guan, Y. (2014). Combined effects of the Pacific decadal oscillation and the El-Niño-Southern Oscillation on global land dry-wet changes. *Scientific Reports 4*(1), 1-8.

Weare, B. (2013). El Niño teleconnections in CMIP5 models, *Climate Dynamics, 41(7-8), 2165-2177.*

Yeh, S., Cai, W., Min, S., et al. (2018). ENSO atmospheric teleconnections and their responses to greenhouse gas forcing, *Reviews of Geophysics, 56(1), 185-206.*

Zhai, P., Yu, R., Gou, Y., et al. (2016). The strong El Niño of 2015/16 and its dominant impacts of global and China's climate, *Journal of Meteorological Research, 30(3), 283-297.*